Gold Bulletin (2023) 56:83–96
https://doi.org/10.1007/s13404-023-00334-2

RESEARCH

Drug release properties of amphoteric HES/p(AETAC-co-IA) hydrogels decorated with gold nanoparticles

Merve Ilkiner[1] · **Ozgur Ozay**[2]

Received: 20 May 2023 / Accepted: 5 September 2023 / Published online: 16 September 2023

Abstract

In this study, amphoteric hydroxyethyl starch/p([2(acryloyloxy)ethyl]trimethylammonium chloride-co-itaconic acid (HES/p(AETAC-co-IA) hydrogels containing both cationic and anionic groups in their structure were synthesized by the redox polymerization method. The synthesized hydrogels were modified with gold nanoparticles, and nanocomposite hydrogels were obtained. The characterizations of the nanocomposite HES/p(AETAC-co-IA)@Au hydrogels prepared for biomedical applications were carried out by SEM, TEM, FT-IR, TGA, and XRD techniques and swelling tests in simulated biological environments. Hydrogels designed as drug carrier cargo materials were loaded with sodium diclofenac (NaDcF) and ibuprofen drugs, and their release properties were studied. The release mechanisms and release kinetics of the two drugs were studied. The release kinetics determined for the drug NaDcF is consistent with the Higuchi model, while the release kinetics determined for ibuprofen is consistent with the first-order model. In addition, the antibacterial and antifungal properties of the hydrogels were tested. It was found that the HES/p(AETAC-co-IA)@Au hydrogel was effective against gram-positive *Staphylococcus aureus*, gram-negative *Pseudomonas aeruginosa*, and the fungal species *Candida albicans*.

Keywords Hydrogel · Drug delivery · Nanocomposite · Gold nanoparticle · Antibacterial material

Introduction

Medicines at the right time and in the right dose play an important role in curing diseases. Traditional methods involve the use of high doses of drugs and a repetitive cycle. In controlled drug release systems, the drug is given at the required dose and at the specified rate [1]. The main advantage of controlled drug release systems is that the drug can be delivered to the target region at the right dose and at the right rate. This increases the efficacy of the treatment by avoiding toxicity of the drug [2]. For these reasons, there has been a recent increase in interest in controlled drug delivery systems. With this increasing interest, the research and development of biomaterials that can be used as drug delivery systems are coming to the forefront. Hydrogels are the main class of materials that have recently been used in the literature as controlled drug delivery systems. In addition to hydrogels, materials such as dendrimers [3], nanoparticles [4], metallic nanoparticles [5], nanospheres [6], and microgels [7, 8] are also used for drug delivery in drug delivery systems.

Hydrogels are hydrophilic, covalently bonded polymers with a cross-linked network structure. Due to hydrogen bonds and van der Waals interactions between their main chains, they are insoluble in water. In this way, they can adsorb large amounts of water. Moreover, they have a high storage capacity for adsorbed molecules [9]. These properties are the result of swelling behavior due to the interaction of the macromolecular chains with the solvent molecules. Hydrogels, which are also called superabsorbent materials, can reach a weight several hundred times their own weight due to the action of water molecules [10].

Synthetic hydrogels are usually not biodegradable. The natural polymer added to the structure transforms the hydrogel into a biodegradable and biocompatible material [11]. The natural polymer hydroxyethyl starch (HES) has many properties such as cost efficiency, biocompatibility,

✉ Ozgur Ozay
ozgurozay@comu.edu.tr

[1] Laboratory of Biopolymers, Department of Bioengineering and Materials Engineering, School of Graduate Studies, Çanakkale Onsekiz Mart University, Çanakkale, Turkey

[2] Laboratory of Biopolymers, Department of Bioengineering, Faculty of Engineering, Çanakkale Onsekiz Mart University, Çanakkale, Turkey

biodegradability, high absorption capacity, and non-toxicity. Thanks to the interaction of hydroxyl groups in its structure with different functional groups, new properties can be imparted to the hydrogel by changing the chemical properties of its surface. This fact expands the fields of application of HEPP [12]. [2-(Acryloyloxy)ethyl]trimethylammonium chloride (AETAC) is an important cationic monomer containing the quaternary ammonium salt group. It is a unique monomer for adsorption of molecules with anionic groups due to its cationic property [13]. Itaconic acid (IA) is an anionic monomer derived from biomass. Therefore, it can adsorb cationic molecules through electrostatic interactions. Itaconic acid is produced by fermentation of carbohydrates such as glucose and molasses with fungi such as *Aspergillus terreus* and *Aspergillus itaconicus*. It is a monomer with excellent properties for hydrogels that can be used in biomedical applications due to its biodegradability [14].

Cationic hydrogels, which are to be used to transport ionic drugs to tissues in the body, have unique properties for biomedical applications. These hydrogels can adsorb large amounts of water and have a flexible structure [1]. Basic cationic hydrogels with a positive charge exhibit swelling behavior at low pH due to ionization and electrostatic repulsion. These hydrogels can respond to external factors and exhibit antibacterial properties [15]. Antibacterial hydrogels attack and destroy the cell membrane of microorganisms. In this way, they do not cause any possible side effects or toxicity. Due to these advantages, they can be used instead of antibiotic drugs that harm the human body [16]. The swelling behavior of negatively charged anionic hydrogels depends on the pH of the external environment. Amphoteric hydrogels contain both cationic and anionic groups in their structure. The swelling behavior of these hydrogels varies depending on the content of anionic and cationic groups [17].

Hydrogels can be prepared as composites with different inorganic materials, making them more mechanically durable. In addition, new functional groups and properties can be added to the structure [18]. By combining hydrogels and metal materials, hydrogel-metal composite structures have emerged. These structures have attracted a lot of attention in recent years. This is because metals provide advantages such as antibacterial properties, biocompatibility, and biodegradability to the synthesized hydrogel due to their large surface areas [19].

In this study, a HES/p(AETAC-co-IA) hydrogel system with amphoteric and hydrophilic properties was synthesized using the cationic monomer AETAC, the anionic monomer IA, and the natural polymer HES. A biocomposite material was prepared by modifying the network structures of the synthesized hydrogel with gold nanoparticles. The resulting amphoteric hydrogel composites were used for the controlled release of NaDcF and ibuprofen drugs used to reduce the inflammatory process and pain. The resulting percent drug release of HES/p(AETAC-co-IA) hydrogels released 98% and 100% of the active ingredients NaDcF and ibuprofen, respectively. For HES/p(AETAC-co-IA)@Au hydrogels, the cumulative release values for NaDcF and ibuprofen were found to be 33.85% and 95%, respectively. In addition, the hydrogels showed antibacterial properties against *Pseudomonas aeruginosa*, *Staphylococcus aureus*, and *Candida albicans* bacteria and fungi.

Material and methods

Materials

The used monomers for the synthesis of hydrogels, [2(acryloyloxy)ethyl]trimethylammonium chloride (AETAC, 80 wt. % in H_2O), itaconic acid (IA, 99%) ve hydroxyethyl starch (HES), N,N′-methylenebis(acrylamide) (MBA, 99%) used as cross-linker, N,N,N′,N′-tetramethylethylenediamine (TEMED, 99%) used as catalyst, and ammonium persulfate (APS, 99.9%) used as initiator were purchased from Sigma-Aldrich chemical company. Potassium gold (III) chloride (99%) used for the preparation of hydrogel composites, sodium diclofenac (99%), and ibuprofen (98%) used in controlled-release studies were obtained from Sigma-Aldrich. Tryptic soy agar (TSA) and tryptic soy broth (TSB) were purchased from Merck for antimicrobial studies. Deionized water, simulated body fluid (SBF pH = 7.4), simulated salivary fluid (SSF, pH = 7.4), simulated intestinal fluid (PBS, pH = 7.0), isotonic NaCl (0.9%, pH = 7.0), and simulated gastric juice (SGF, pH = 2.2) buffer solutions used for swelling characterizations of hydrogels were prepared according to literature, and deionized water was used in the all solutions [20, 21]. All experiments conducted were performed triplicate in the study.

Synthesis of HES/p(AETAC-co-IA) hydrogels and composites

Hydrogels were synthesized by the cross-linking reaction of polymer chains and redox polymerization methods [1, 20, 21]. For the synthesis of hydrogel HES/p(AETAC-co-IA), 95% mol of AETAC and 5% IA monomers were used. For the synthesis, AETAC (4.75 mmol) and IA (0.25 mmol) were taken and homogeneously mixed, and 0.5 mL of HES solution with a concentration of 25 mg/mL was added to the monomer mixture. Cross-linker (MBA) (0.059 mmol) was added to the homogeneously mixed monomer mixture at a ratio of 0.5% according to the total number of monomer mole. Then, 40 µL of TEMED was added to the reaction medium as an accelerator. The reaction was started by adding 0.5 mL of APS (1% (0.05 mmol) of the total amount of

monomer by mole) dissolved in 0.5 mL of ultra-deionized water to the resulting mixture. The resulting reaction mixture was transferred to plastic pipettes with a diameter of 0.3 cm to bring it into shape, and it waited for 12 h for the polymerization reaction to complete. After this time, the hydrogels were removed from the pipette and cut to an average size of 0.3 cm × 0.5 cm. The resulting hydrogels were washed with 6 × 50 mL of deionized water for 1 day to remove unreacted reagents and dried in a vacuum oven at 50 °C. They were then stored in a desiccator for characterization and drug release studies.

The synthesis yield (Eq. 1) for hydrogels, the gel fraction (Eq. 2) known as the amount of cross-linked polymer, and the sol–gel fraction as the amount of uncross-linked polymer were calculated by gravimetric method (Eq. 3) [22].

$$\text{Yield } \% = [W_c/W_i] \times 100 \quad (1)$$

$$\text{Gel fraction} = [W_d/W_c] \times 100 \quad (2)$$

$$\text{Sol} - \text{gel fraction} = 100 - \text{gel fraction} \quad (3)$$

Here, W_c is the dry weight after synthesis; W_i is the total weight of the monomers, and W_d is the mass of the hydrogel that has been washed and dried after the synthesis, with the impurities removed.

For the synthesis of gold nanoparticles stabilized in hydrogel network structures of HES/p(AETAC-co-IA), 50 mg of dried hydrogel was added to the gold ion solution at a concentration of 250 mg/L (25 mL). It was expected with a period of 24 h for the completion of the adsorption of $[AuCl_4]^-$ ions. After this period, the hydrogels, which were removed from the gold (III) solution and washed with deionized water, were transferred to 0.5 M ascorbic acid solution (100 mL) for the reduction process, and the reduction process was waited for 6 h. The hydrogels that exhibited black coloration were removed from the solution at the end of the time (Fig. 1). Then, the hydrogels washed with deionized water were used for controlled drug release and antibacterial testing.

Characterization of hydrogels

The chemical constituents of the hydrogels were analyzed using FT-IR analysis (Perkin Elmer, Spectrum 100 instrument with ATR apparatus in the wavelength range of 650–4000 cm^{-1}). The surface morphology of HES/p(AETAC-co-IA) hydrogel was studied using the scanning electron microscope (SEM) QUANTA FEG 250 model instrument. Transmission electron microscopy (TEM) (JEOL JEM -1400 PLUS (Tokyo, Japan)) and XRD (PANalytical Empyrean) were used to characterize the Au nanoparticles synthesized in the hydrogels. Thermogravimetric analyzes of hydrogel and hydrogel-metal composite structures were performed using TGA (Perkin ELMER TGA 8000 (USA)) at a heating rate of 10 °C/min. For controlled drug release, a PG instruments T80+ UV-Vis spectrophotometer (UK) (NaDcF: λ_{max} = 276 nm, ibuprofen λ_{max} = 264 nm) was used to determine drug concentrations.

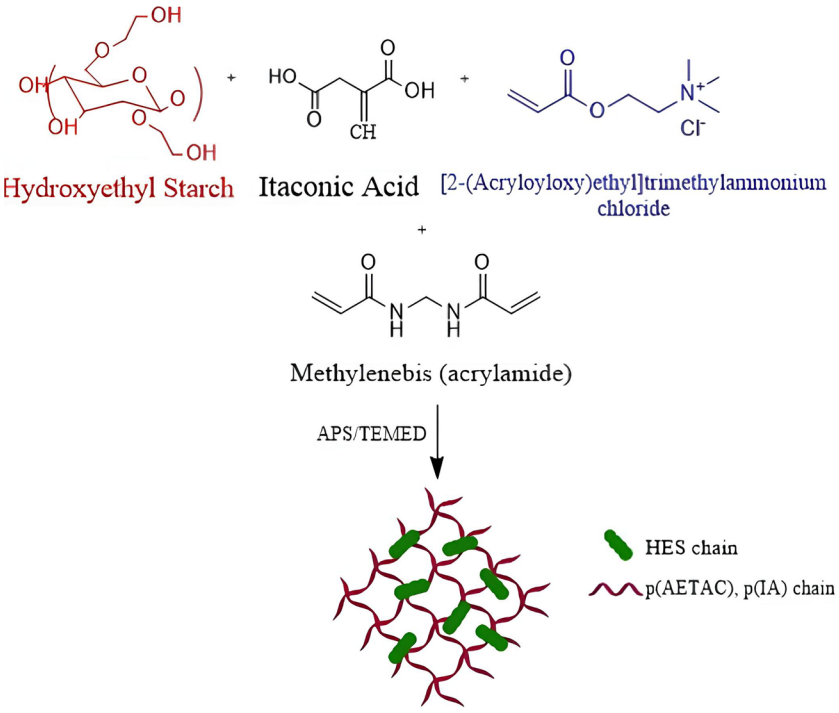

Fig. 1 Schematic representation of the synthesis of HES/p(AETAC-co-IA) hydrogels

The swelling of HES/p(AETAC-co-IA) hydrogels was characterized in 50 mL of PBS, SGF, SSF, SBF, isotonic liquid, and deionized water. Equilibrium swelling amounts were determined gravimetrically by recording the masses of the hydrogels at specific times [23]. The formula for calculating the equilibrium swelling was given in Eq. 4, where M_0 is the dry mass of the hydrogels, M_t is the swollen mass of hydrogels, and St % is the percentage of swelling [24–26]. The swelling amounts of hydrogels containing ionizable groups in their structure were determined in different pH environments for pH = 2, 4, 6, 8, 10, and 12. For this purpose, the hydrogel with known dry mass was added to the solution and waited for 24 h. Then, the maximum swelling value (Eq. 4) was calculated for the hydrogel that had reached the equilibrium swelling value.

$$\text{St } \% = [(M_t - M_0)/M_0] \times 100 \quad (4)$$

Drug loading and release studies from HES/p(AETAC-co-IA) hydrogels

In the drug loading and release studies to hydrogel and hydrogel@Au composite, NaDcF and ibuprofen were used as model drugs. The drugs were dissolved in deionized water, and a drug solution was prepared at a concentration of 250 mg/L (50 mL). A hydrogel or hydrogel@Au composite with an average mass of 50 mg was added to the prepared solution. It took 18 h for the hydrogels to complete drug loaded. The drug-loaded hydrogels were then transferred to PBS release medium (30 mL). At specific time intervals until the release process was completed, the absorbance values of the environment were measured using a UV-Vis spectrophotometer, and the amount of release was calculated. Each drug release was repeated three times, and the results were averaged.

Antimicrobial activity tests

Disk diffusion method was used in antibacterial tests using fungi, gram-negative, and gram-positive bacteria in order to examine the antibacterial activity of HES/p(AETAC-co-IA) and HES/p(AETAC-co-IA)@Au composite hydrogels [27]. For this purpose, *Pseudomonas aeruginosa* (ATCC 27853) was selected as gram-negative bacteria, *Staphylococcus aureus* (ATCC 29213) as gram-positive bacteria, and *Candida albicans* (ATCC 90028) as fungus. Colonies in the culture medium were suspended in TSB medium to propagate the bacteria. The medium was stirred at 37 °C at 100 rpm for 15 h; 25 µL of the bacterial suspension was homogeneously distributed into Petri dishes prepared with tryptic soy agar using a sterile swab. The drug-free, NaDcF-loaded ibuprofen-loaded forms of hydrogels and composites were cut into slices 10 mm in diameter and 0.5-cm wide. The slices were placed opposite to each other on the surface of the medium containing the bacterial suspension. The prepared Petri dishes were incubated at 37 °C for 15 h. At the end of the 15 h, the inhibition diameters were measured to determine the antibacterial activities of the hydrogels.

Results and discussion

Hydrogels are cross-linked polymers consisting of linear polymer chains connected by cross-links. Thanks to the hydrophilic groups in their structure, they can absorb large amounts of water. Therefore, they have a physical similarity to human tissue, which has a high percentage of water in

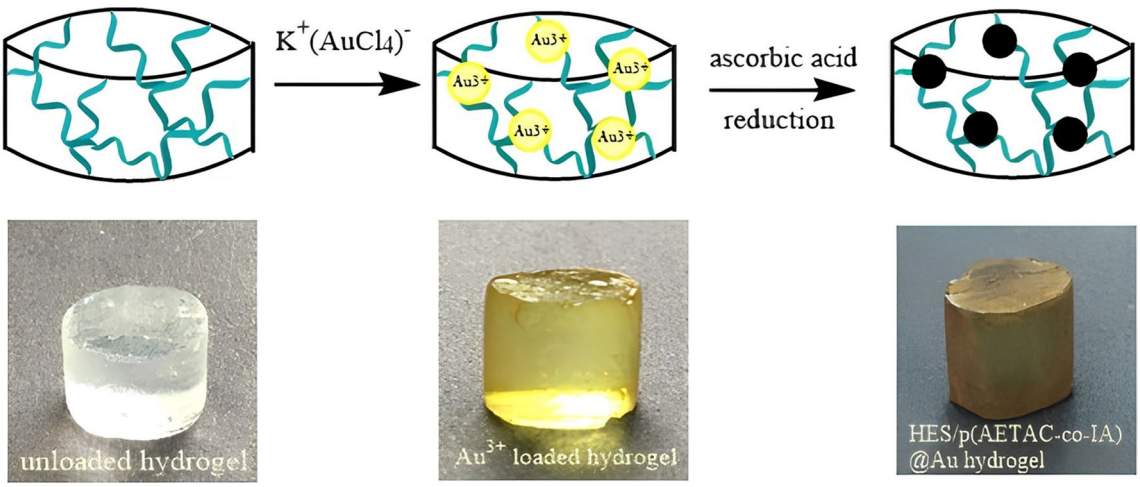

Fig. 2 Digital camera images of the synthesis of HES/p(AETAC-co-IA)@Au nanocomposite hydrogels

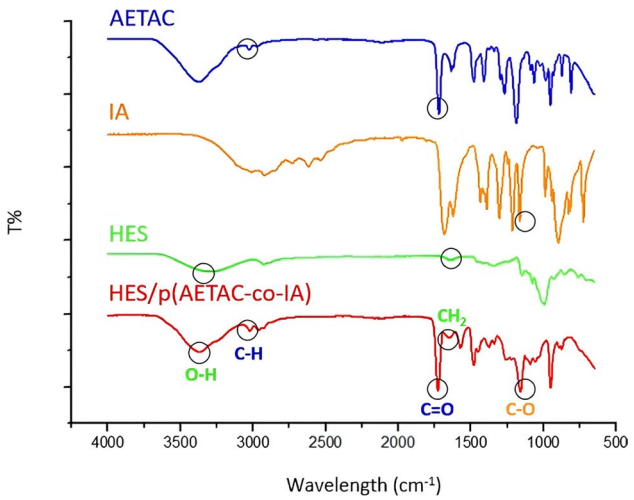

Fig. 3 FT-IR spectra of HES/p(AETAC-co-IA) hydrogels

its structure [28]. In addition, hydrogels are biocompatible and have a high drug absorption capacity. Thanks to the cross-linked polymer network, the hardness of the hydrogel can also be adjusted. This gives the hydrogel numerous mechanical properties [29]. The functional groups of the monomers in the hydrogel structure can impart anionic or cationic properties to the hydrogels. Thanks to the anionic or cationic groups in their structure, hydrogels can be designed for different applications. In this study, an amphoteric HES/p(AETAC-co-IA) hydrogel with both anionic and cationic groups in its structure was synthesized by redox polymerization. The scheme of hydrogel synthesis is shown in Fig. 1. IA in the structure of the hydrogel designed for biomedical applications was used to impart an anionic character to the hydrogel, and AETAC was used to impart a cationic character to the hydrogel network structure. MBA was used as a cross-linker, and APS was used as initiator in the synthesis of hydrogels. HES which is used for the biocompatible and biodegradable properties of the structure is a natural polymer. The hydrogels were prepared in the form of cylindrical disks to investigate the potential for drug delivery. The values for the yield, gel, and sol-gel in the synthesis of hydrogels containing cross-linker at a ratio of 2% based on the total moles of monomer were 89.99%, 82.03%, and 17.97%, respectively.

Gold is a metal that is frequently preferred for biomedical applications with its biocompatible and biodegradable properties, as well as effective against bacteria and viruses [30]. At the same time, it is known that metallic nanoparticles prepared in nanoscale are more active thanks to their high surface areas. However, the biggest challenge in preparing nanosized metals is the high surface energies of nanometals. Therefore, nanometallic particles tend to agglomerate [31]. In this study, hydrogel Au nanoparticles were prepared in combination with an amphoteric hydrogel network by in situ reduction method. Thanks to the hydrogel network structures, the gold nanoparticles were stabilized while the hydrogel gained additional biocompatibility and antibacterial properties [32]. The synthesis scheme of Au nanoparticles synthesized in hydrogel network structures was shown in Fig. 2. According to Fig. 2, the hydrogel was added to the gold (III) solution. Thanks to the cationic groups in the hydrogel structure, the $[AuCl_4]^-$ ions in the network structures of the hydrogels, which hold the $[AuCl_4]^-$ ions with electrostatic interactions, were reduced with ascorbic acid. In this way, HES/p(AETAC-co-IA)@Au composites were obtained. The Au nanoparticles in the obtained network structure

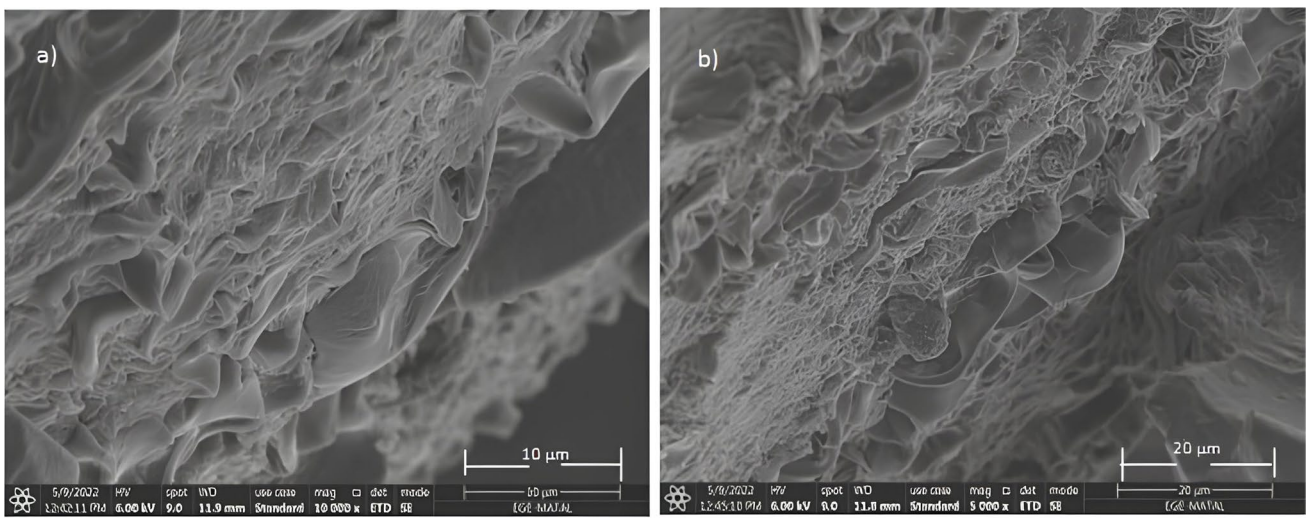

Fig. 4 SEM images of HES/p(AETAC-co-IA) hydrogels

of the hydrogel composite remained stable thanks to the cross-links and had no tendency to agglomerate.

The FT-IR analysis performed to determine the presence of HES, IA, and AETAC molecules in the hydrogel network is shown in Fig. 3. Examining the FT-IR spectra of the hydrogel and the individual components, the 952 cm^{-1} peak shows the C–N stretching vibrations of the ammonium groups of the AETAC monomer; the 1720 cm^{-1} peak shows the C=O stretching of the ester group, and the 2960 and 3025 cm^{-1} peaks show the symmetric and asymmetric C–H stretching vibrations of the methylene groups [33]. The peak at 1683 cm^{-1} observed in the FT-IR spectrum of IA shows the C=O stretching, while 1154 cm^{-1} represents the peak of the C–O stretching vibration [34]. In the spectrum of HES, the O–H stretching vibration signal of hydroxyl groups in the broad peak structure at 3294 cm^{-1} and the signal at 1645 cm^{-1} indicates the C–H bending vibration signal of methylene groups (CH_2) [24]. In the FT-IR spectrum of HES/p(AETAC-co-IA) hydrogels, the O–H stretching of the hydroxyl and carboxylic acid groups

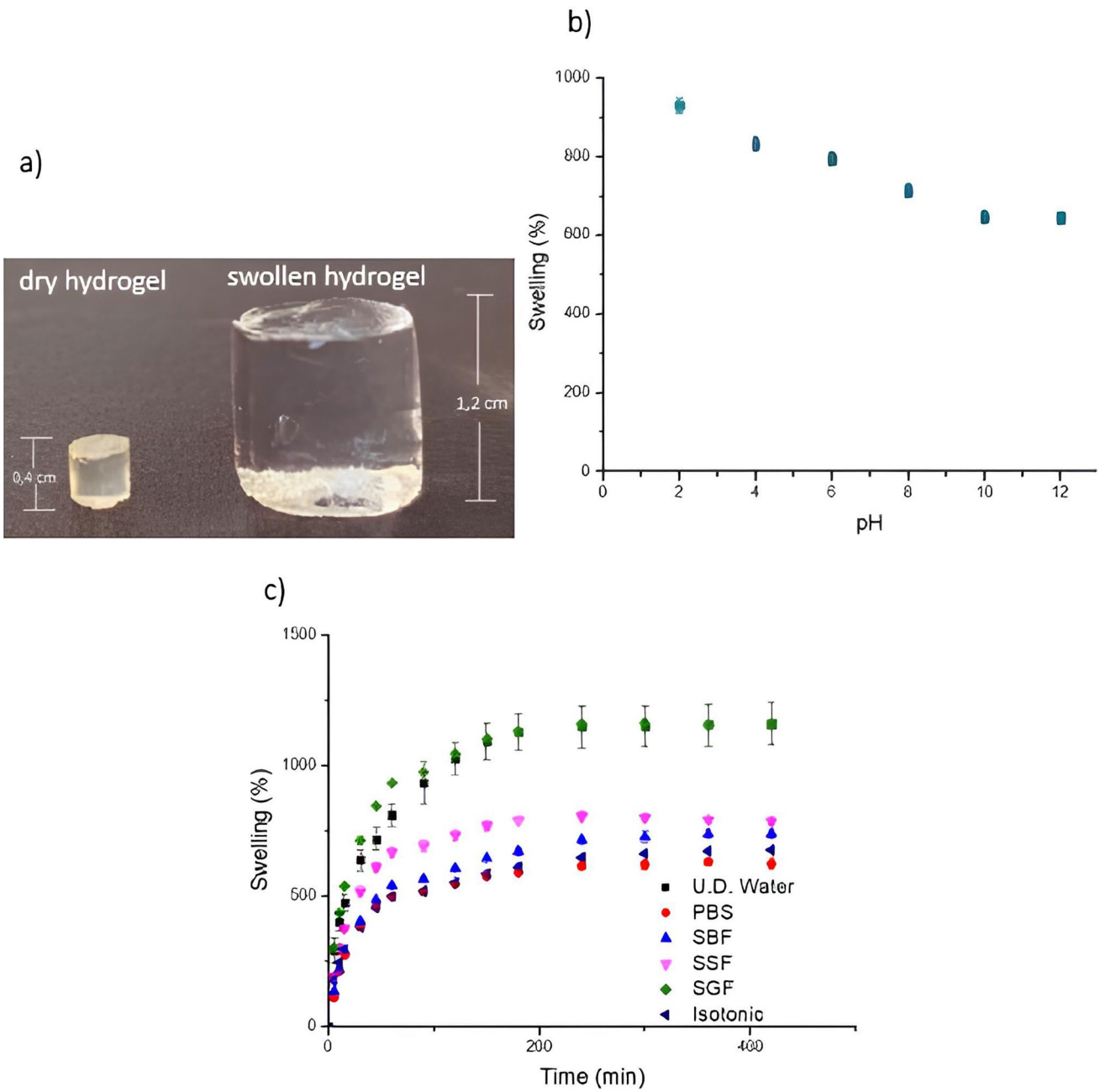

Fig. 5 **a** Digital camera images of dry and swollen hydrogels, **b** pH dependence **c** in various environments swelling isotherms of the hydrogels

Table 1 Diffusion parameters of HES/p(AETAC-co-IA) hydrogels

Swelling media	S_{max}	k_0	r_0	n	k	D
Deionized water	1250	1.9×10^{-7}	3.3	0.434	0.2902	2.670
PBS	666.6	4.5×10^{-3}	2.0	0.682	0.0599	602.5
SBF	769.2	3.4×10^{-3}	2.0	0.608	0.1385	0.003
SSF	833.3	4.8×10^{-3}	3.3	0.615	0.1269	349.1
SGF	1250	3.2×10^{-3}	5.0	0.479	0.1297	1620
Isotonic fluid	714.3	3.9×10^{-3}	2.0	0.430	0.2513	797.9

shows a broad signal structure centered at 3371 cm^{-1}. The signal from the carboxylic acid and ester functional groups of IA and AETAC was observed as a single coincident intensity peak at 1727 cm^{-1}. The fact that all the characteristic peaks of the components in the structure of the hydrogel were observed in the spectrum of FT-IR indicates that the hydrogel was successfully synthesized.

The high absorption capacity of a hydrogel is directly related to the hydrophilicity of its functional groups and the porosity of the network structure. Thanks to these pores, water and drug molecules dissolved in water can easily diffuse into the hydrogel. Solvent molecules that penetrate into the network structure of the hydrogel in the release medium can easily transport the drug into the tissue [35]. To study the morphological structure of HES/p(AETAC-co-IA) hydrogels, they were kept in deionized water until the swelling equilibrium value was reached at maximum capacity. Then, the structure of the hydrogel network was prevented from collapse by removing the adsorbed water with the hydrogel lyophilized and freezing the hydrogel at −20 °C. The hydrogels were analyzed by SEM after coating with Au. SEM images of the hydrogel are shown in Fig. 4. By examining Fig. 4, the network structure and porous structure of the hydrogel can be seen. The pores are on average 1–5 µm in size. The porous structure of the hydrogel surface provides additional advantages for solvent diffusion and thus for drug loading and release phases.

Hydrogels exhibit different swelling behaviors in biological environments due to dissolved molecules in different solution environments. The swelling behavior is also closely related to the ratio of cross-linkers, pore size, and chemical structure. In order to desorb the drug molecules, which are held by electrostatic interaction mainly thanks to the functional groups in the hydrogels, the biological fluids must penetrate the hydrogel. This is possible by filling the hydrogel with liquid as a result of osmotic pressure. Thus, the applications of hydrogels can be diversified depending on the swelling behavior [33–37]. Figure 5a shows digital camera photographs of the HES/p(AETAC-co-IA) hydrogels in the dry and maximum swollen states. The maximum water holding capacity of HES/p(AETAC-co-IA) hydrogel containing biopolymer in its structure and synthesized as pH sensitive smart material was determined at different pH values. For this purpose, 6 different solutions with pH = 2, 4, 6, 8, 10, and 12 were used. The pH values of the solutions were adjusted with 0.1 M HCl and 0.1 M NaOH solutions. The maximum swelling values are shown in Fig. 5b. The maximum swelling values of the hydrogels in the range pH = 2–12 were determined to be 930.7%, 833.3%, 795.2%, 714.5%, 646.7%, and 644.2%, respectively. The higher water retention in acidic media is compatible with the hydrogels containing 95% AETAC and 5% by mol IA. In this case, the highest swelling rate is obtained because the more concentrated positive charges in the hydrogel structure repel each other. At the same time, the formation of sodium salts of the acid groups of itaconic acid in basic medium explains the

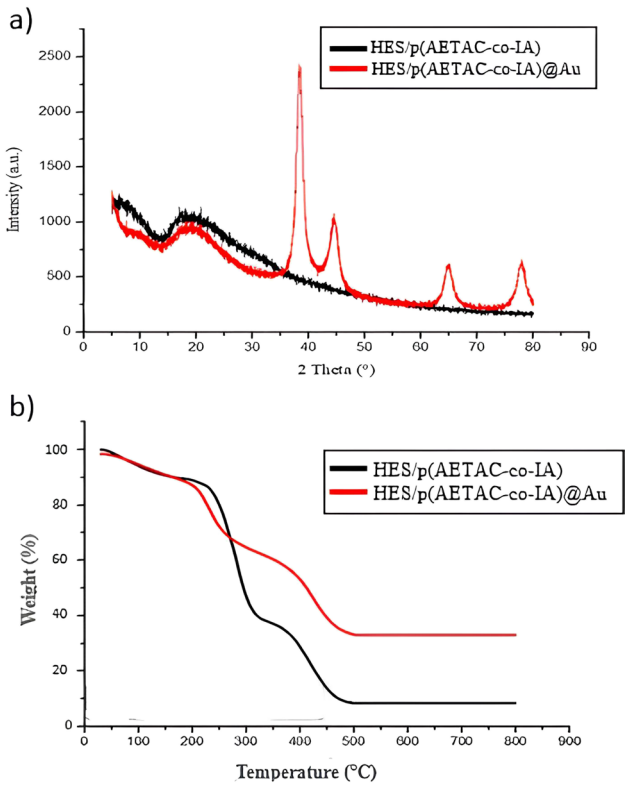

Fig. 6 **a** XRD spectrum and **b** TGA microgram of HES/p(AETAC-co-IA)@Au nanocomposite hydrogels

swelling of the hydrogel with a minimum rate of 644.2% by mass.

Swelling of HES/p(AETAC-co-IA) hydrogels in potential drug release environments was performed in six different environments. These media were selected to study the swelling properties of hydrogels in liquid media in the living body. Intestinal medium (PBS), salivary medium (SSF), gastric (SGF), body fluid (SBF), and isotonic have the same pH as serum fluid. Thus, the properties of drug release in organs or fluids in the living body have been studied.

HES/p(AETAC-co-IA) hydrogel was stored in deionized water, PBS, SBF, SSF, SGF, and isotonic liquid media for approximately 420 min. The mass of the hydrogel was measured at specific time intervals over 420 min. The swelling values obtained are shown in Fig. 5c. The maximum swelling ratios in mass percent for the hydrogel

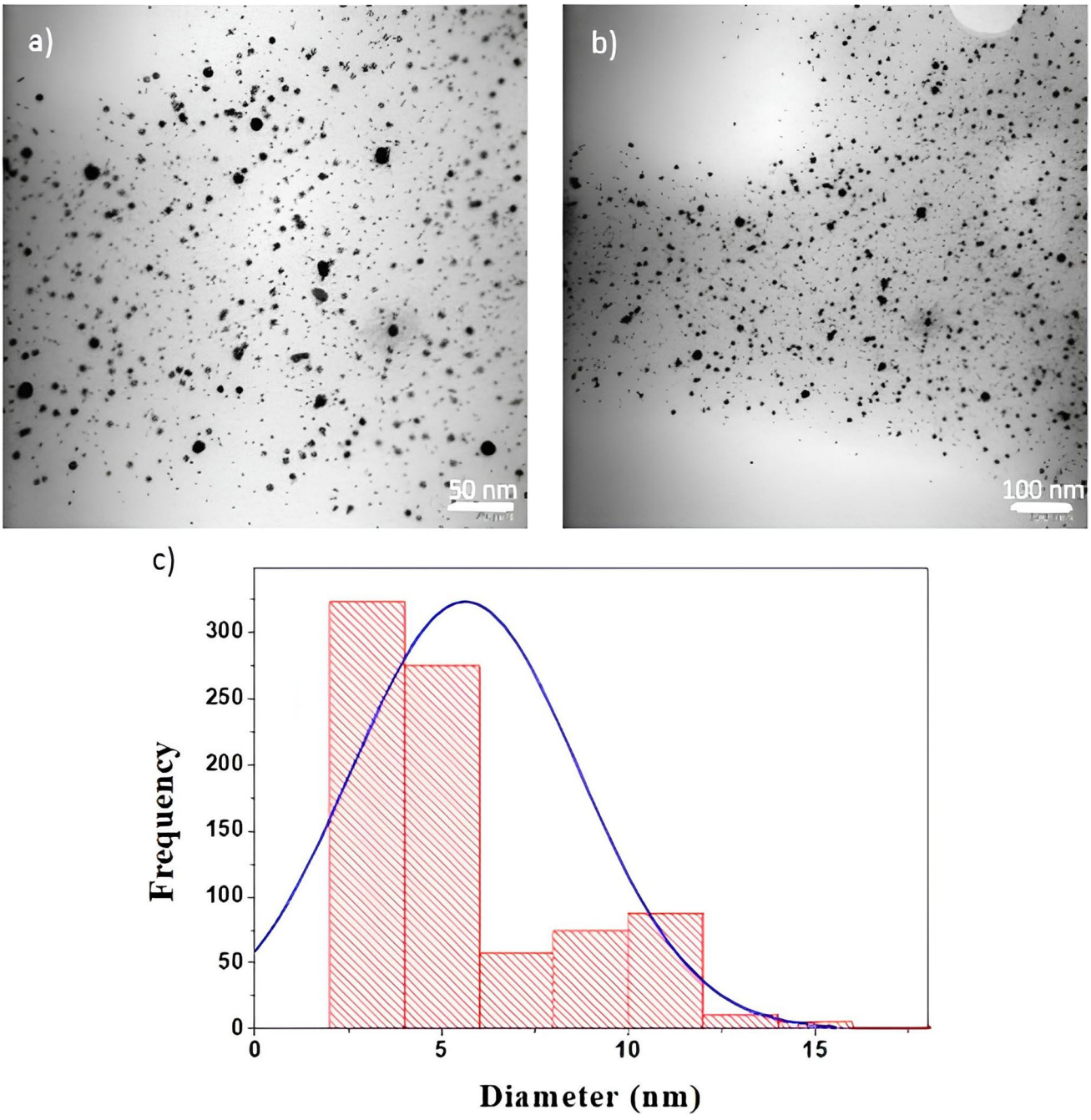

Fig. 7 **a**, **b** TEM images of HES/p(AETAC-co-IA)@Au nanocomposite hydrogels at different magnifications and **c** particle size distribution graph of gold nanoparticles in the HES/p(AETAC-co-IA)@Au hydrogel

HES/p(AETAC-co-IA) are 1161.9% in deionized water, 633.1% in PBS, 741.4% in SBF, 806.6% in SSF, 1162.2% in SGF, and 678.5% in isotonic medium. It is observed that the hydrogel swells more in deionized water and SGF environments than in other media. The reason for the high swelling behavior in deionized water is that it does not contain ions. The reason for the high swelling behavior in the SGF environment is the electrostatic interactions between the positively charged ammonium groups (C–N) in the HES/p(AETAC-co-IA) hydrogel and the H^+ ions in the SGF environment. As a result, the hydrogel exhibits high swelling behavior [38].

The Korsmeyer-Peppas model was used for the swelling kinetics of the hydrogel HES/p(AETAC-co-IA). The kinetic parameter values obtained for the hydrogel are given in Table 1. The r_0 given in Table 1 represents the initial swelling rate; k_0 represents the swelling rate that determines the rate constant, and S_{max} represents the equilibrium swelling rate. These data were obtained by plotting t/s against t. The n values indicate whether the swells in the environments are of Fick's diffusion type. Values of n greater than 0.45 are referred to as non-Fickian diffusion type, while values less than 0.45 are referred to as Fickian diffusion type. The n values were found to be 0.434, 0.682, 0.608, 0.615, 0.479, and 0.430 for deionized water, PBS, SBF, SSF, SGF, and isotonic liquids, respectively. From these data, it can be seen that they are suitable for Fick's diffusion type for deionized water and isotonic liquids. For the media PBS, SBF, SSF, and SGF, they seem to correspond to the non-Fickian diffusion type [39].

Metallic nanoparticles such as Ag and Au stabilized by any matrix can generally be prepared in the crystalline phase because they do not clump together. The XRD diffraction pattern of the synthesized HES/p(AETAC-co-IA)@Au composites, which impart additional antibacterial properties to the structure of the hydrogels, is shown in Fig. 6a. According to Fig. 6a, the hydrogel of HES/p(AETAC-co-IA) has an amorphous structure. This can be seen from the broad peak with an angle of 2θ, which occurs in the range of 10–30°. The peak in the XRD pattern of the HES/p(AETAC-co-IA)@Au composite hydrogel, which occurs in the same region, is from the hydrogel. However, in addition to this peak in the XRD spectrum of the HES/p(AETAC-co-IA)@Au composite hydrogel, the peaks of 38.5°, 44.9°, 65.1°, and 77.9° observed in the face-centered cubic (FCC) gold (111), (200) , (220), and (311) correspond to the crystal planes [36, 37]. These results demonstrate the existence of crystalline gold nanoparticles, known for their biocompatibility, in the network structure of the HES/p(AETAC-co-IA) hydrogel.

Nanocomposite hydrogels containing metallic nanoparticles show a different degradation profile curve than non-composite hydrogels. Hydrogels with Au nanoparticles in their structure are more temperature resistant than empty hydrogels. The TGA spectra of the hydrogels and hydrogel@Au composites are shown in Fig. 6b. The thermal properties of HES/p(AETAC-co-IA) and HES/p(AETAC-co-IA)@Au hydrogels were investigated under nitrogen atmosphere in the temperature range from 30 to 900 °C (10 °C/min). Examination of the TGA curve for the HES/p(AETAC-co-IA) hydrogel shows that it exhibits 4 different decomposition temperatures. The initial decomposition occurred due to free and bound moisture in the range of 0–250 °C with a mass loss of 13%. In the second decomposition step, a mass loss of 48% was observed in the range of 250–325 °C, and in the third decomposition step, a mass loss of 29% was observed in the range of 325–500 °C. In the fourth degradation phase of the HES/p(AETAC-co-IA) hydrogel, a mass loss of 10% is observed in the range 500–800 °C. However, when the TGA curve for the HES/p(AETAC-co-IA)@Au hydrogel, we find that it exhibits four different decomposition temperatures. The first decomposition step occurred in the range of 0–200 °C due to free and bound moisture, with a mass loss of 13%. The second decomposition step

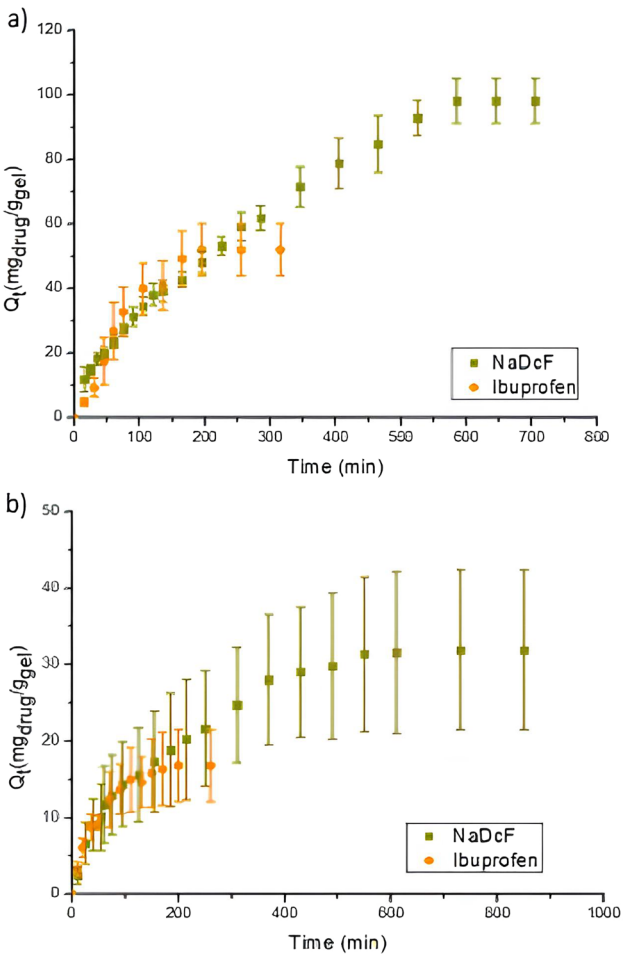

Fig. 8 Release of NaDcF and İbuprofen from the hydrogels **a** HES/p(AETAC-co-IA) and **b** HES/p(AETAC-co-IA)@Au

showed an 18% mass degradation in the narrower temperature range of 200–260 °C compared to the non-composite hydrogel. The third degradation step caused a 37% mass loss in the 260–500 °C range. The last degradation step of the HES/p(AETAC-co-IA)@Au composite hydrogel shows a 32% mass degradation in the range of 500–800 °C. The difference of 27.3% by mass between the two spectra is the amount of Au synthesized in the hydrogel network structure.

TEM images of Au nanoparticles synthesized in a hydrogel network structure are given in Fig. 7. According to these images, the hydrogel network structures acted as a good stabilizing barrier. As shown in Fig. 7, the Au nanoparticles are almost homogeneously distributed in the HES/p(AETAC-co-IA)@Au nanocomposite hydrogel. This image also proves that the AETAC monomer, which adsorbs $[AuCl_4]^-$ ions by electrostatic interactions, is homogeneously distributed in the hydrogel. The particle size distribution diagram of the nanoparticles shown in Fig. 7c was again obtained using the Image J program. Here, it can be seen that the Au nanoparticles also have a nearly monodisperse size distribution and an average diameter of 7 nm.

Characterization of the hydrogels HES/p(AETAC-co-IA) and hydrogel@Au composites showed that the hydrogels were suitable for controlled drug release studies. NaDcF and ibuprofen drugs were loaded into HES/p(AETAC-co-IA) hydrogel and hydrogel@Au composites for controlled drug release studies. Controlled release studies were then performed in PBS medium. The release graphs for the HES/p(AETAC-co-IA) hydrogel are shown in Fig. 8a, and the release graphs for the HES/p(AETAC-co-IA)@Au hydrogel are shown in Fig. 8b. The time-dependent release values of the NaDcF hydrogel were measured with a UV-Vis spectrophotometer over a period of approximately 700 min to ensure controlled release of the drug release. The maximum adsorption amount for the NaDcF drug of the HES/p(AETAC-co-IA) hydrogel was determined to be 91.13 mg_{drug}/g_{gel} (cumulative release 98%). In contrast, the hydrogel containing the ibuprofen drug released 52.07 mg_{drug}/g_{gel} (cumulative release 100%), which it held for 200 min.

The HES/p(AETAC-co-IA)@Au nanocomposite hydrogel adsorbed the NaDcF and ibuprofen drugs 31.95 mg_{drug}/g_{gel} and 16.85 mg_{drug}/g_{gel}, respectively. The reason why composite hydrogels adsorb less drug than empty hydrogels is because the Au nanoparticles in their structure reduce the number of active groups adsorbing drugs in the hydrogel. Composite hydrogels contain 27.3% by mass of Au nanoparticles. The cumulative release value obtained as a result of the release experiments performed in PBS medium is 33.85% at the end of 730 min for the NaDcF drug, while it is 95% at the end of 200 min for the ibuprofen drug.

In order to determine the parameters related to the release kinetics and to determine with which model the drug release

Table 2 NaDcF and ibuprofen release kinetic parameters of HES/p(AETAC-co-IA) and HES/p(AETAC-co-IA)@Au hydrogels

Hydrogel	Drug	Model name	k	r^2
HES/p(AETAC-co-IA)	NaDcF	Korsmeyer-Peppas	0.7158	0.9804
		Zero-order	8.9118	0.9482
		Higuchi model	0.2335	0.9926
		First-order	−0.1488	0.9486
		Hixson-Crowell	0.3109	0.9903
	Ibuprofen	Korsmeyer-Peppas	0.8896	0.9632
		Zero-order	15.912	0.8719
		Higuchi model	0.1772	0.9858
		First-order	−0.2493	0.9869
		Hixson-Crowell	0.5409	0.9840
HES/p(AETAC-co-IA)@Au	NaDcF	Korsmeyer-Peppas	0.6056	0.9735
		Zero-order	2.7224	0.8727
		Higuchi model	0.7078	0.9810
		First-order	−0.015	0.9030
		Hixson-Crowell	0.0493	0.8934
	Ibuprofen	Korsmeyer-Peppas	1.1699	0.9897
		Zero-order	35.021	0.8496
		Higuchi model	0.1169	0.9751
		First-order	−0.5419	0.9960
		Hixson-Crowell	1.1883	0.9754

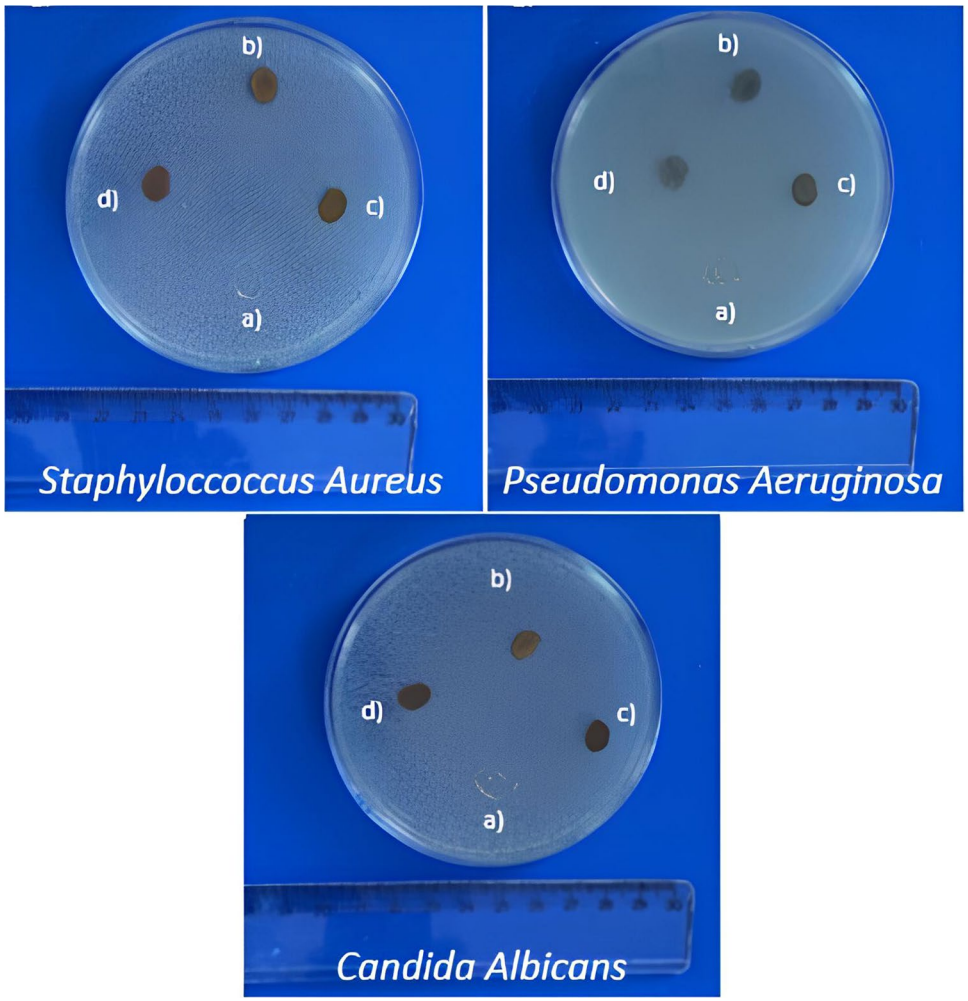

Fig. 9 Digital camera images of antibacterial activity tests of hydrogels and hydrogel@Au nanocomposites for *Staphylococcus aureus*, *Pseudomonas aeruginosa*, and *Candida albicans* (**a**) bare hydrogel, (**b**) hydrogel@Au nanocomposite, (**c**) NaDcF loaded hydrogel, and (**d**) ibuprofen loaded hydrogel

is compatible, the models for each drug carrier hydrogel were studied separately [40, 41]. The equation of the Higuchi model, with which the hydrogels are compatible, was applied to determine the release kinetics parameters of the NaDcF drug. Again, the compatible first-order model equation for the release of ibuprofen from the hydrogels HES/p(AETAC-co-IA) and HES/p(AETAC-co-IA)@Au was applied. The release rate constant (k) and regression (r^2) values obtained from the equations are shown in Table 2. It was found that the release kinetics of the NaDcF drug conformed to the Higuchi model for both hydrogels, whereas the release kinetics of the ibuprofen drug conformed to the first-order model.

Many bacteria have started to become resistant and are getting stronger day by day. Given the danger to human health, much research is being done to prevent resistance. These researches are generally related to natural biomolecules and synthetic antibacterial agents, antimicrobial peptides, chitosan, antibacterial enzymes, graphene, silver, carbon-based materials, and polymers [42]. In the antibacterial mechanisms of cationic compounds, cationic moieties adsorb to phosphate groups of bacterial cell membranes via electrostatic interactions, while hydrophobic segments

Table 3 The inhibition zone radius (cm) of HES/p(AETAC-co-IA) hydrogels and hydrogel@Au nanocomposites

	Bare hydrogel	NaDcF loaded hydrogel	Ibuprofen loaded hydrogel	Hydrogel@Au composite
S. aureus	1.1 ± 0.06	1.1 ± 0.05	1.1 ± 0.05	1.2 ± 0.09
P. aeruginosa	1.1 ± 0.08	1.1 ± 0.08	1.1 ± 0.09	1.2 ± 0.12
C. albicans	1.1 ± 0.09	1.1 ± 0.07	1.1 ± 0.07	1.2 ± 0.08

penetrate into hydrophobic regions of cell membranes and cause the release of cytoplasmic components (RNA, DNA, K+, etc.) and death of bacterial cells. Compared to low molecular weight biocides based on cationic compounds, cationic polymers are attracting more and more attention due to their lower toxicity and better antibacterial properties [43, 44]. The antibacterial activities of the HES/p(AETAC-co-IA) hydrogel against gram-positive *Staphylococcus aureus*, gram-negative *Pseudomonas aeruginosa*, and *Candida albicans* bacteria are shown in Fig. 9. The diameter of the hydrogels used to test antibacterial activity is 1 cm. The zone diameters of the HES/p(AETAC-co-IA) hydrogel, which is drug-free, drug-loaded, and made of a gold nanocomposite, against bacteria are shown in Table 3. By examining Table 3, it was found that the HES/p(AETAC-co-IA) hydrogel showed antibacterial activity for each condition. However, the zone diameter of the drug-free hydrogel containing ibuprofen and NaDcF was 1.1 cm, while the zone diameter of the gold nanocomposite hydrogel was 1.2 cm. As a result of these results, the hydrogel HES/p(AETAC-co-IA) shows antibacterial activity under all conditions. However, the fact that the hydrogels containing Au nanoparticles have higher antibacterial activity than the empty hydrogels shows that the antibacterial properties can be improved by synthesizing the hydrogel structures as Au composites [45].

Conclusions

In this study, an amphoteric HES/p(AETAC-co-IA) hydrogel containing both anionic and cationic monomers was synthesized. The synthesized amphoteric hydrogel was then assembled with Au nanoparticles. The swelling kinetics of the synthesized hydrogel and hydrogel@Au composites was determined, and their structural characterization was carried out by the methods FT-IR, SEM, XRD, TGA, and TEM. The synthesized and characterized hydrogel structures were tested as cargo materials for the model drugs NaDcF and ibuprofen. NaDcF and ibuprofen were released from hydrogel networks for about 700 min and 200 min, respectively. Moreover, the release of NaDcF in hydrogels with the determined release kinetics is consistent with the Higuchi model, while the release of ibuprofen is consistent with the first-order model. As a result of the antibacterial tests conducted for the drug-loaded and non-drug-loaded forms of hydrogel and hydrogel@Au composites, it was found that the hydrogels exhibited antibacterial activity against *S. aureus, P. aeruginosa,* and *Candida albicans*. It was found that Au nanoparticles synthesized into the hydrogel network structure increased the antibacterial property of the hydrogel.

Acknowledgements This study was produced from the master thesis of Merve İlkiner.

Author contribution Merve İlkiner: experimental studies, data processing, and writing. Ozgur Ozay: experimental studies, data processing, writing, and project management. All authors reviewed the manuscript.

Funding This research was funded by the Çanakkale Onsekiz Mart University (FYL-2021-3854).

Declarations

Competing interests The authors declare no competing interests.

References

1. Durmus S, Ozay O (2022) Synthesis and characterization of methacrylic acid based amphoteric hydrogels: use as a dual drug delivery system. J Macromol Sci A 59:646–656. https://doi.org/10.1080/10601325.2022.2107933
2. Lee JS, Nah H, Moon HJ, Lee SJ, Heo DN, Kwon IK (2020) Controllable delivery system: a temperature and pH-responsive injectable hydrogel from succinylated chitosan. Appl Surf Sci 528:146812. https://doi.org/10.1016/j.apsusc.2020.146812
3. Wu LP, Ficker M, Christensen JB, Trohopoulos PN, Moghimi SM (2015) Dendrimers in medicine: therapeutic concepts and pharmaceutical challenges. Bioconjugate Chem 26:1198–1211. https://doi.org/10.1021/acs.bioconjchem.5b00031B
4. Tan RS, Naruchi K, Amano M, Hinou H, Nishimura SI (2015) Rapid endolysosomal escape and controlled intracellular trafficking of cell surface mimetic quantum-dots-anchored peptides and glycopeptides. ACS Chem Biol 10:2073–2086. https://doi.org/10.1021/acschembio.5b00434
5. Yilmaz B, Ozay O (2022) Synthesis of antibiotic-modified silica nanoparticles and their use as a controlled drug release system with antibacterial properties. Phosphorus Sulfur Silicon Relat Elem 197:964–972. https://doi.org/10.1080/10426507.2022.2049267
6. Mitchell MJ, Billingsley MM, Haley RM, Wechsler ME, Peppas NA, Langer R (2021) Engineering precision nanoparticles for drug delivery. Nat Rev 20:101–124. https://doi.org/10.1038/s41573-020-0090-8
7. Kim J (2015) Development of polyethylene glycol-sebacic acid diacrylate microgels as a drug delivery system. Polym Korea 39:677–682. https://doi.org/10.7317/pk.2015.39.4.677
8. Soares DCF, Domingues SC, Viana DB (2020) Polymer-hybrid nanoparticles: current advances in biomedical applications. Biomed Pharmacother 131:110695. https://doi.org/10.1016/j.biopha.2020.110695
9. Ahmed EM (2015) Hydrogel: Preparation, characterization, and applications: a review. J Adv Res 6:105–121. https://doi.org/10.1016/j.jare.2013.07.006
10. Wang HY, Heilshorn SC (2015) Adaptable hydrogel networks with reversible linkages for tissue engineering. Adv Mater 27:3717–3736. https://doi.org/10.1002/adma.201501558
11. Jiang G, Qiu W, DeLuca PP (2003) Preparation and in vitro/in vivo evaluation of insulin-loaded poly(acryloyl-hydroxyethyl starch)-PLGA composite microspheres. Pharm Res 20:452–459. https://doi.org/10.1023/A:1022668507748
12. Ilgin P, Ozay H, Ozay O (2020) The efficient removal of anionic and cationic dyes from aqueous media using hydroxyethyl starch-based hydrogels. Cellulose 27:4787–4802. https://doi.org/10.1007/s10570-020-03074-0
13. Onder A, Ilgin P, Ozay H, Ozay O (2020) Removal of dye from aqueous medium with pH-sensitive poly[2-(acryloyloxy)ethyl]

trimethylammonium chloride-co-1-vinyl-2-pyrrolidone cationic hydrogel. J Environ Chem Eng 8:104436. https://doi.org/10.1016/j.jece.2020.104436
14. Hong SJ, Kwon YR, Lim SH, Kim JS, Choi J, Chang YW, Kim DH (2021) Improved absorption performance of itaconic acid based superabsorbent hydrogel using vinyl sulfonic acid. Polym-Plast Tech Mat 60:1166–1175. https://doi.org/10.1080/25740881.2021.1888982
15. Cao B, Tang C, Li L, Mutevazi J, Wu H, Liu L, Ceng C (2013) Switchable antimicrobial and antifouling hydrogels with enhanced mechanical properties. Adv Healthc Mater 2:1096–1102. https://doi.org/10.1002/adhm.201200359
16. Kundu R, Payal P (2020) Antimicrobial hydrogels: promising soft biomaterials. ChemistrySelect 5:14800–14810. https://doi.org/10.1002/slct.202003666
17. Kharlampieva E, Unal IE, Sukhishvili SA (2007) Amphoteric surface hydrogels derived from hydrogen-bonded multilayers: reversible loading of dyes and macromolecules. Langmuir 23:175–181. https://doi.org/10.1021/la061652p
18. Tan HL, Teow SY, Pushpamalar J (2019) Application of metal nanoparticle–hydrogel composites in tissue regeneration. Bioengineering 6:17. https://doi.org/10.3390/bioengineering6010017
19. Ahmedian Z, Geybi H, Adeli M (2022) Efficient wound healing by antibacterial property: advances and trends of hydrogels, hydrogel-metal NP composites and photothermal therapy platforms. J Drug Deliv Sci Technol 73:103458. https://doi.org/10.1016/j.jddst.2022.103458
20. Durmus S, Yilmaz B, Onder A, Ilgin P, Ozay H, Ozay O (2022) An innovative approach to use zeolite as crosslinker for synthesis of p(HEMA-co-NIPAM) hydrogel. Monatsh fur Chem 153:369–382. https://doi.org/10.1007/s00706-022-02908-w
21. Ozay O (2013) Synthesis and swelling behavior of novel pH responsive hydrogels for environmental applications. Polym Plast Technol Eng 53:130–140. https://doi.org/10.1080/03602559.2013.843697
22. Ganguly S, Das CN (2015) Synthesis of a novel pH responsive phyllosilicate loaded polymeric hydrogel based on poly(acrylic acid-co-N-vinylpyrrolidone) and polyethylene glycol for drug delivery: modelling and kinetics study for the sustained release of an antibiotic drug. Rsc Adv 5:18312–18327. https://doi.org/10.1039/C4RA16119J
23. Ozay H, Ozay O (2013) Rhodamine based reusable and colorimetric naked-eye hydrogel sensors for Fe^{3+} ion. Chem Eng J 232:364–371. https://doi.org/10.1016/j.cej.2013.07.111
24. Ozay O, Ilgin P, Ozay H, Gungor Z, Yilmaz B, Kivanc MR (2020) The preparation of various shapes and porosites of hydroxyethyl starch/p(HEMA-co-NVP) IPN hydrogels as programmable carrier for drug delivery. J Macromol Sci A 57:379–387. https://doi.org/10.1080/10601325.2019.1700803
25. Ozay O, Ozay H (2014) Synthesis and characterization of drug microspheres containing phosphazene for biomedical applications. Colloids Surf A Physicochem Eng Asp 450:99–105. https://doi.org/10.1016/j.colsurfa.2014.03.022
26. Ozay H, Sahin O, Koc OK, Ozay O (2016) The preparation and applications of novel phosphazene crosslinked thermo and pH responsive hydrogels. J Ind Eng Chem 43:28–35. https://doi.org/10.1016/j.jiec.2016.07.043
27. Ilgin P, Zorer OS, Ozay O, Boran G (2017) Synthesis and characterization of 2-hydroxyethylmethacrylate/2-(3-indol-yl) ethylmethacrylamide-based novel hydrogels as drug carrier with in vitro antibacterial properties. J Appl Polym Sci 134:45550. https://doi.org/10.1002/app.45550
28. Caló E, Khutoryanskiy VV (2015) Biomedical applications of hydrogels: a review of patents and commercial products. Eur Polym J 65:252–267. https://doi.org/10.1016/j.eurpolymj.2014.11.024
29. Fuchs S, Shariati K, Ma M (2019) Specialty tough hydrogels and their biomedical applications. Adv Healthc Mater 9:1901396. https://doi.org/10.1002/adhm.201901396
30. Durmuş S, Yilmaz B, Kıvanç MR, Onder A, Ilgin P, Ozay H, Ozay O (2021) Synthesis, characterization, and in vitro drug release properties of AuNPs/p(AETAC-co-VI)/Q nanocomposite hydrogels. Gold Bull 54:75–87. https://doi.org/10.1007/s13404-021-00295-4
31. Ilgin P, Ozay O, Ozay H (2019) A novel hydrogel containing thioether group as selective support material for preparation of gold nanoparticles: synthesis and catalytic applications. Appl Catal B 241:415–423. https://doi.org/10.1016/j.apcatb.2018.09.066
32. Chitra G, Franklin DS, Sudarsan S, Sakthivel M, Guhanathan S (2018) Noncytotoxic silver and gold nanocomposite hydrogels with enhanced antibacterial and wound healing applications. Polym Eng Sci 58:2133–2142. https://doi.org/10.1002/pen.24824
33. Onder A, Kivanc MR, Ilgin P, Ozay H, Ozay O (2023) Synthesis of p(HEMA-co-AETAC) nanocomposite hydrogel with vinyl-function montmorillonite nanoparticles and effective removal of methyl orange from aqueous solution. J Macromol Sci A 60:108–123. https://doi.org/10.1080/10601325.2023.2169155
34. Erbil C, Uyanik N (2001) Interactions between poly(acrylamide)-poly(itaconic acid) and cerium(IV)-nitrilotriacetic acid redox pair in the synthesis of acrylamide and itaconic acid homo- and copolymers. Polym Int 50:792–795. https://doi.org/10.1002/pi.697
35. Kim SJ, Lee CK, Lee YM, Kim IY, Kim SI (2003) Electrical/pH-sensitive swelling behavior of polyelectrolyte hydrogels prepared with hyaluronic acid-poly(vinyl alcohol) interpenetrating polymer networks. React Funct Polym 55:291–298. https://doi.org/10.1016/S1381-5148(03)00019-1
36. Singh J, Kumar S, Dhaliwal AS (2020) Controlled release of amoxicillin and antioxidant potential of gold nanoparticles-xanthan gum/poly (acrylic acid) biodegradable nanocomposite. J Drug Deliv Sci Tec 55:101384. https://doi.org/10.1016/j.jddst.2019.101384
37. Ozay H, Tarimeri N, Gungor Z, Demirbakan B, Ozcan B, Sezginturk MK, Ozay O (2020) A new approach to synthesis of highly dispersed gold nanoparticles via glucose oxidase-immobilized hydrogel and usage in the reduction of 4-nitrophenol. ChemistrySelect 5:9143–9152. https://doi.org/10.1002/slct.202002327
38. Shaghaleh H, Hamoud YA, Xu X, Liu H, Wang S, Sheteiwy M, Dong F, Qian Y, Li P, Zhang S (2021) Thermo-/pH-responsive preservative delivery based on TEMPO cellulose nanofiber/cationic copolymer hydrogel film in fruit packaging. Int J Biol Macromol 183:1911–1924. https://doi.org/10.1016/j.ijbiomac.2021.05.208
39. Ferrer C, Massuelle D, Doelker E (2010) Towards elucidation of the drug release mechanism from compressed hydrophilic matrices made of cellulose ethers. II. Evaluation of a possible swelling-controlled drug release mechanism using dimensionless analysis. J Control Release 141:223–233. https://doi.org/10.1016/j.jconrel.2009.09.011
40. England CG, Miller MC, Kuttan A, Trent JO, Frieboes HB (2015) Release kinetics of paclitaxel and cisplatin from two and three layered gold nanoparticles. Eur J Pharm Biopharm 92:120–129. https://doi.org/10.1016/j.ejpb.2015.02.017

41. Rizzello L, Pompa PP (2014) Nanosilver-based antibacterial drugs and devices: mechanisms, methodological drawbacks and guidelines. Chem Soc Rev 43:1501–1518. https://doi.org/10.1039/c3cs60218d
42. Yuan H, Yu B, Fan L, Wang M, Zhu Y, Ding X, Xu F (2016) Multiple types of hydroxyl-rich cationic derivatives of PGMA for broad-spectrum antibacterial and antifouling coatings. Polym Chem 7:5709–5718. https://doi.org/10.1039/C6PY01242F
43. Guo J, Qin J, Ren Y, Wang B, Cui H, Ding Y, Yan F (2018) Antibacterial Activity of cationic polymers: side-chain or main-chain type? Polym Chem 9:4611–4616. https://doi.org/10.1039/c8py00665b
44. Chen J, Wang F, Liu Q, Du J (2014) Antibacterial polymeric nanostructures for biomedical applications. Chem Commun 50:14482–14493. https://doi.org/10.1039/C4CC03001J
45. Grace AN, Pandian K (2007) Antibacterial efficacy of aminoglycosidic antibiotics protected gold nanoparticles-a brief study. Colloids Surf A Physicochem Eng Asp 297:63–70. https://doi.org/10.1016/j.colsurfa.2006.10.024